Dalton Transactions

RSC Publishing

PAPER

View Article Online
View Journal | View Issue

Cite this: *Dalton Trans.*, 2013, **42**, 10198

A coumarin-based "turn-on" fluorescent sensor for the determination of Al^{3+}: single crystal X-ray structure and cell staining properties†

Subarna Guha,[a] Sisir Lohar,[a] Animesh Sahana,[a] Arnab Banerjee,[a] Damir A. Safin,*[b] Maria G. Babashkina,[b] Mariusz P. Mitoraj,*[c] Michael Bolte,[d] Yann Garcia,[b] Subhra Kanti Mukhopadhyay[e] and Debasis Das*[a]

Received 20th April 2013,
Accepted 8th May 2013

DOI: 10.1039/c3dt51045j

www.rsc.org/dalton

An efficient Al^{3+} receptor, 6-(2-hydroxybenzylideneamino)-2*H*-chromen-2-one (**HBC**), has been synthesized by condensing salicylaldehyde with 6-aminocoumarin. The molecular structure of **HBC** has been determined by a single crystal X-ray analysis. It was established that in the presence of Al^{3+}, **HBC** shows 25 fold enhancement of fluorescence intensity which might be attributed to the chelation-enhanced fluorescence (CHEF) process. **HBC** binds $Al(NO_3)_3$ in a 1 : 1 stoichiometry with a binding constant (*K*) of 7.9×10^4 M^{-1}. Fe^{3+} and Mn^{2+} quench the emission intensity of the [**HBC** + Al^{3+}] system to an insignificant extent at a concentration 10 times higher compared to that of Al^{3+}. **HBC** is highly efficient in the detection of intracellular Al^{3+} under a fluorescence microscope.

Introduction

Aluminum (Al) is the third most prevalent and abundant metal in the earth's crust. Leaching of Al from soil during acid rain increases free Al^{3+} which is deadly to growing plants.[1] Al has already been identified as a neurotoxin.[2] According to the World Health Organization (WHO) the average daily human intake of Al is ~3–10 mg. Tolerable weekly Al dietary intake in the human body is estimated to be 7 mg kg^{-1} body weight.[3] Recently, evidence that ingested Al additives contained in processed foods and alum-treated drinking water are a major risk factor for Alzheimer's disease has been discussed.[4,5] Furthermore, Al might be responsible for Parkinson's disease, osteomalacia[6] and also for breast cancer.[7] It is also responsible for the intoxication in hemodialysis patients.[8] It is not an essential element for biological life and, hence, its high concentration in a body can cause harm to the brain and kidneys.[9,10] Al has widespread application in industry, packaging materials, electrical equipment, food additives, clinical drugs, drinking water supplies, water purification, computers and many others.[11–13] However, the detection of Al^{3+} has always been problematic due to the lack of spectroscopic characteristics and poor coordination ability compared to transition metals.[14,15] Recently, the fluorescent method has become popular due to its operational simplicity, high selectivity, sensitivity, rapidity, nondestructive methodology and direct visual perception.[16] For an efficient fluorescent sensor, in addition to a high selectivity towards an ion, a significant change in the fluorescence intensity in the presence of an ion and/or a spectral change are required.[17,18]

On the other hand, several metal complexes with Schiff bases[19] have antitumor properties,[20] antioxidative activities[21] and attractive electronic and photophysical properties.[22] The use of a fluorescence technique for the trace level detection of Al^{3+} sensor is becoming very popular and the volume of contributions in this field is rising exponentially.[23–28] Recently, several Al^{3+} selective "turn-on" fluorescent probes derived from hydrazone,[29] Schiff bases,[30] coumarin,[31] pyrollidine,[32] calixarene,[33] boron dipyrromethene,[34] hydroxyflavone,[35] 8-hydroxyquinoline,[36] oxazoline and imidazoline,[37] and bipyridyl-dansyl[38] have been reported. Most of them have suffered at least from one of the following parameters: cost of synthesis, the number of synthesis steps, selectivity, LOD, detection medium, binding constant, crystal structure of a probe and

[a]*Department of Chemistry, The University of Burdwan, Burdwan, 713104 West Bengal, India. E-mail: ddas100in@yahoo.com; Fax: +91 342 2530452; Tel: +91 342 2533913*
[b]*Institute of Condensed Matter and Nanosciences, Molecules, Solids and Reactivity (IMCN/MOST) – Université Catholique de Louvain, Place L. Pasteur 1, 1348 Louvain-la-Neuve, Belgium. E-mail: damir.safin@ksu.ru; Fax: +32 (0) 1047 2330; Tel: +32 (0) 1047 2831*
[c]*Department of Theoretical Chemistry, Faculty of Chemistry, Jagiellonian University, R. Ingardena 3, 30-060 Cracow, Poland. E-mail: mitoraj@chemia.uj.edu.pl*
[d]*Institut für Anorganische Chemie J.-W.-Goethe-Universität, Frankfurt/Main, Germany*
[e]*Department of Microbiology, The University of Burdwan, Burdwan 713104, India*
†Electronic supplementary information (ESI) available: Tables S2 and S3. CCDC 857625. For ESI and crystallographic data in CIF or other electronic format see DOI: 10.1039/c3dt51045j

applications.[25,26,32,36,39–45] Recently, we have also reported on the ratiometric fluorescence sensing and intracellular imaging of Al^{3+} with a pyrimidine–pyrene scaffold.[46] However, the described sensor also suffers from the cost of the starting materials and requires coordination of the two ligands to Al^{3+} to enhance turn-on fluorescence.

To overcome most of these limitations, herein we report a very cheap Al^{3+} selective "turn-on" fluorescent probe 6-(2-hydroxybenzylideneamino)-2*H*-chromen-2-one (**HBC**) derived from 6-aminocoumarin and salicylaldehyde in a facile single step. **HBC** can detect intra-cellular Al^{3+} in the contaminated living cell under a fluorescence microscope.

Results and discussion

The compound **HBC** was synthesized by reacting 6-amino-coumarin with the salicylaldehyde in methanol to afford a yellow crystalline solid (Scheme 1). Reaction of **HBC** with $Al(NO_3)_3$ in methanol leads to the formation of the deep yellow **[Al(HBC)-(MeOH)$(NO_3)_3$]** complex (Scheme 1).

The FTIR spectrum of **HBC** contains bands for the C=N, C=O and OH groups at 1624, 1724, 3427 cm^{-1}, respectively (Fig. S1 in ESI†). The same bands in the FTIR spectrum of **[Al(HBC)(MeOH)$(NO_3)_3$]** were observed at 1615, 1724 and 3423 cm^{-1}, respectively (Fig. S2 in the ESI†). While the band for the C=O group remains constant, the bands for the C=N and OH groups slightly shift to low frequencies. This might testify to a coordination of the metal cation through the imine nitrogen and hydroxyl oxygen atoms of the parent ligand **HBC** in the solid state. Besides, the FTIR spectrum of **[Al(HBC)-(MeOH)$(NO_3)_3$]** also contains an intense band for the NO_3 group at 1385 cm^{-1}.

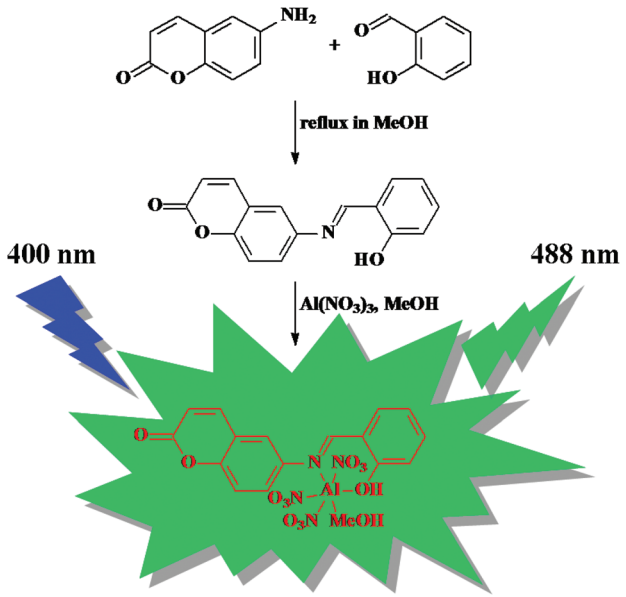

Scheme 1 Preparation of **HBC** and **[Al(HBC)(MeOH)$(NO_3)_3$]**.

In order to support the binding of Al^{3+} with the receptor **HBC**, the ^1H NMR titrations have been performed in a mixture of D_2O–CD_3OD = 7 : 3 (v/v) (Fig. 1). The ^1H NMR spectrum of **HBC** contains signals for the CHN and aryl fragments at 10.0

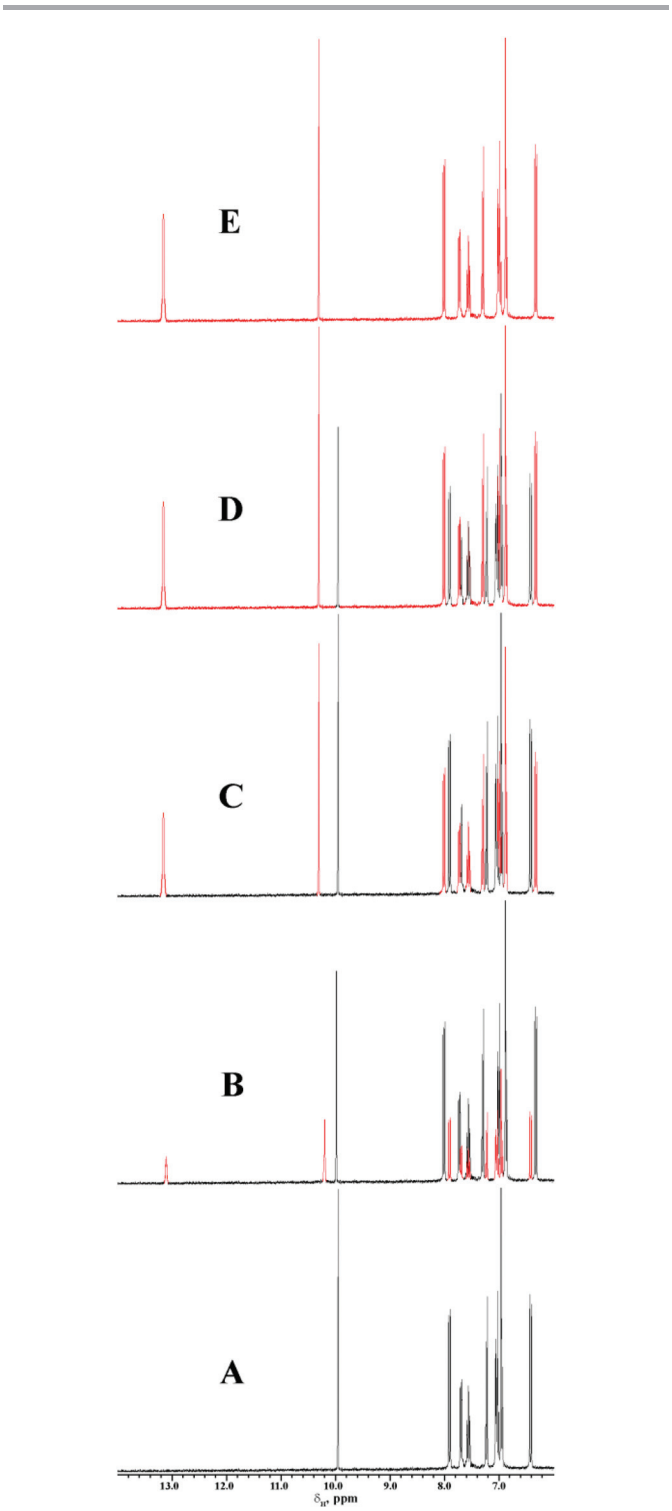

Fig. 1 ^1H NMR titration of **HBC** by $Al(NO_3)_3{\cdot}9H_2O$ in D_2O–CD_3OD = 7 : 3 (v/v): (A) **HBC**; (B) **HBC** + 0.5 equivalent of Al^{3+}; (C) **HBC** + 1 equivalent of Al^{3+}; (D) **HBC** + 2 equivalents of Al^{3+}; (E) **HBC** + 3 equivalents of Al^{3+}. Signals for the free **HBC** are in black, while the signals for the complex are in red.

and 6.2–8.0 ppm, respectively (Fig. 1, A). It should be noted that the spectrum of **HBC** contains no signals for the OH proton due to a fast exchange with the solvent. Addition of 0.5 equivalent of $Al(NO_3)_3{\cdot}9H_2O$ leads to the appearance of the OH proton signal at about 13 ppm as well as the signal for the CHN proton is 0.2 ppm low-field shifted compared to that in the ^1H NMR spectrum of the parent ligand **HBC** (Fig. 1, B). This testifies to a binding of Al^{3+} by the imine nitrogen and OH oxygen atoms of **HBC**. Furthermore, the signals for the aryl protons are also shifted compared to those in the spectrum of free ligand. Addition of 1 and 2 equivalents of $Al(NO_3)_3{\cdot}9H_2O$ leads to a further gradual increase of the integral intensities of the signals corresponding to the complex (Fig. 1, C and D). At the same time a gradual decrease of the integral intensities of the signals corresponding to the free ligand **HBC** has been observed. Addition of 3 equivalents of Al $(NO_3)_3{\cdot}9H_2O$ results in the exclusive presence of the signals of the complex (Fig. 1, E).

In order to further confirm binding of **HBC** to Al^{3+} we have calculated, based on the DFT/BP86/TZP method, the structure of **[Al(HBC)(NO$_3$)$_3$]** and its ^1H NMR spectrum based on the GIAO approach as implemented in the Amsterdam Density Functional (ADF) package (Fig. S3 in ESI†).[47,48] We have omitted methanol from the coordination sphere of the complex because a mixture of D_2O and CD_3OD has been used in the experiment. Analysis of the **[Al(HBC)(NO$_3$)$_3$]** structure leads to the conclusion that the OH proton in **HBC** has been transferred to the adjacent NO_3 fragment, forming the O_2NO–H···O(**HBC**) intramolecular hydrogen bond (Fig. S3 in the ESI†). This explains the appearance of the OH proton signal at ~13 ppm (Fig. 1). In addition, the theoretical ^1H NMR spectrum of **[Al(HBC)(NO$_3$)$_3$]** confirms that the OH proton signal is located at the lowest-field region (Fig. S3 in the ESI†).

The UV-Vis absorption spectrum of **HBC** in aqueous MeOH contains four bands in the UV region at 240, 277, 318 and 347 nm (Fig. S4 in the ESI†). The former two bands are significantly more intense compared to the latter two bands. The UV-Vis absorption spectrum of **[Al(HBC)(MeOH)(NO$_3$)$_3$]** in the same solvent also exhibits four bands, where the first three bands were observed almost at the same wavelengths (240, 275 and 321 nm) as was observed for **HBC** (Fig. S4 in the ESI†). It should be noted that while the intensity of the band at 240 nm remains constant, intensities of the latter two bands decrease. The absorption band at 347 nm disappeared in the UV-Vis absorption spectrum of **[Al(HBC)(MeOH)(NO$_3$)$_3$]**, while a new band appeared at 375 nm. It is worth noting that further UV-Vis titration of **HBC** by Al^{3+} in aqueous MeOH leads to a gradual increase of the absorption bands at 270, 310 and 386 nm with increasing $[Al^{3+}]$. The former band exhibits a slightly hypsochromic shift compared to the corresponding band in the spectrum of [**HBC** + Al^{3+}] ($\Delta\lambda$ = 5 nm), while the latter band exhibits a bathochromic shift ($\Delta\lambda$ = 11 nm) (Fig. 2).

In order to shed light on the qualitative picture of the absorption in **HBC** and **[Al(HBC)(MeOH)(NO$_3$)$_3$]** species, we have performed TD-DFT calculations (at the B3LYP/TZP level of theory) using the ADF program.[47,48] It can be noticed that

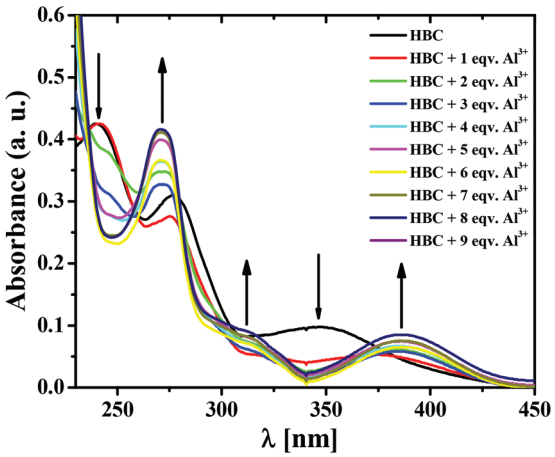

Fig. 2 UV-Vis titration of **HBC** (1 μM) by Al^{3+} in H_2O–MeOH = 7 : 3 (v/v).

the overall shape of the calculated UV-Vis spectrum of **[Al(HBC)(MeOH)(NO$_3$)$_3$]** is similar to the experimental one (Fig. 3, A). The most intense band at 274.3 nm involves predominantly two transitions. The former transition HOMO − 4 → LUMO with the oscillator strength f = 0.4055 a.u. involves a $\pi \rightarrow \pi^*$ charge transfer predominantly within the salicylaldehyde ring, whereas the latter one HOMO − 2 → LUMO + 2 consists of a similar $\pi \rightarrow \pi^*$ transfer but at the coumarin unit (Fig. 3). A less intense peak (f = 0.2380 a.u.) at 367.7 nm is based on the HOMO → LUMO transfer, arising from the

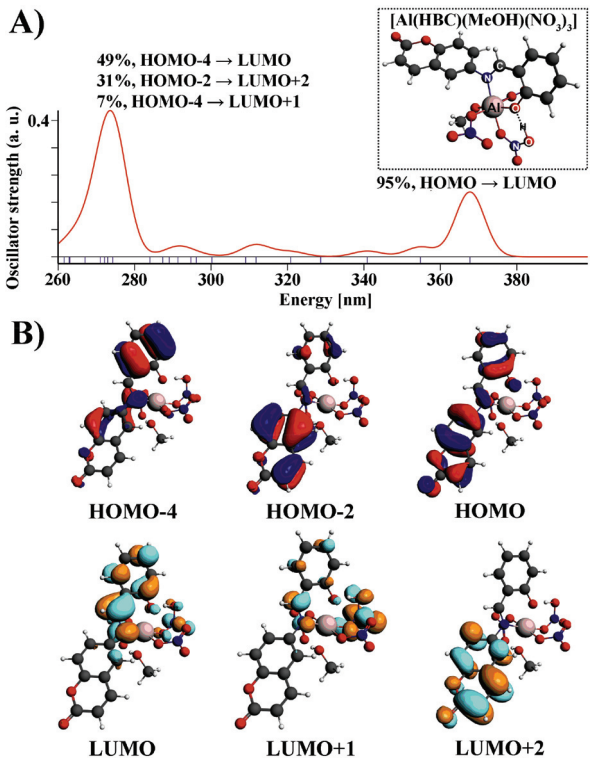

Fig. 3 Simulated TD-DFT absorption spectrum (B3LYP/TZP, gas phase) of **[Al(HBC)(MeOH)(NO$_3$)$_3$]** (A) together with the contours of molecular orbitals involved in the dominant transitions (B).

occupied π orbitals of both fragments (coumarin and salicylaldehyde) to the empty π*, mostly of the salicylaldehyde unit. Similar π → π* based transitions were obtained for **HBC** (Fig. S7 in the ESI†).

The QTOF-MS ES^+ spectrum of **HBC** contains the $[M + Na]^+$ molecular ion peak (Fig. S5 in the ESI†), while the QTOF-MS ES^+ spectrum of **[Al(HBC)(MeOH)(NO$_3$)$_3$]** contains two molecular ion peaks of the following structures: $[M - NO_3]^+$ and $[M + Na]^+$ (Fig. S6 in the ESI†). Furthermore, the mass spectrum of the complex also exhibits peaks for the parent ligand: [**HBC** + $H]^+$, [**HBC** + $Na]^+$ and [**HBC** + $K]^+$. The former two peaks are the most intense in the mass spectrum of the complex. There are also two peaks corresponding to the 6-aminocoumarin: [6-aminocoumarin + $H]^+$ and [6-aminocoumarin + $Na]^+$.

It is well known that the performance of fluorescence sensors based on the electron donor/acceptor mechanism depends largely on the concentration of proton in the medium as it competes with the metal ion of interest for binding the probe. Thus, optimization of pH on the efficiency of the sensor is essential. Fluorescence pH titrations have been carried out for this purpose in aqueous MeOH. Equivalent amounts of **HBC** and Al^{3+} have been taken in different sets of pH (pH 2.2–11.0) (Fig. 4). The fluorescence emission intensity of **HBC** remains unchanged on addition of Al^{3+} at pH below 6.2 and above 9. Most presumably, protonation of **HBC** at pH below 6.2 inhibited it to coordinate Al^{3+}. Over pH 9, competition of OH^- with **HBC** for binding to Al^{3+} succeeded.

Interaction of **HBC** with Al^{3+} has resulted in the fluorescence enhancement at 488 nm (λ_{ex} = 400 nm), which is attributed as chelation-enhanced fluorescence (CHEF). Fig. 5 (top) shows changes in the emission intensities upon gradual addition of Al^{3+} to the **HBC** solution. The plot shown in Fig. 5 (bottom) reveals no further change in the emission intensity of the system over a certain amount of externally added Al^{3+}. We have observed linearity up to 18 equivalents of Al^{3+} (R^2 = 0.9763). This linear part of the plot may be used for the determination of unknown $[Al^{3+}]$ in a sample. Moreover, Al^{3+} has induced a blue shift (about 70 nm) of the emission maximum of **HBC**.

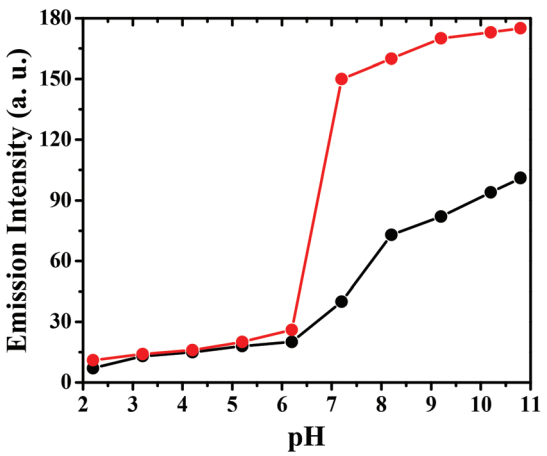

Fig. 4 pH-dependent titration of **HBC** (black) and [**HBC** + Al^{3+}] (red) in H_2O–MeOH = 7 : 3 (v/v).

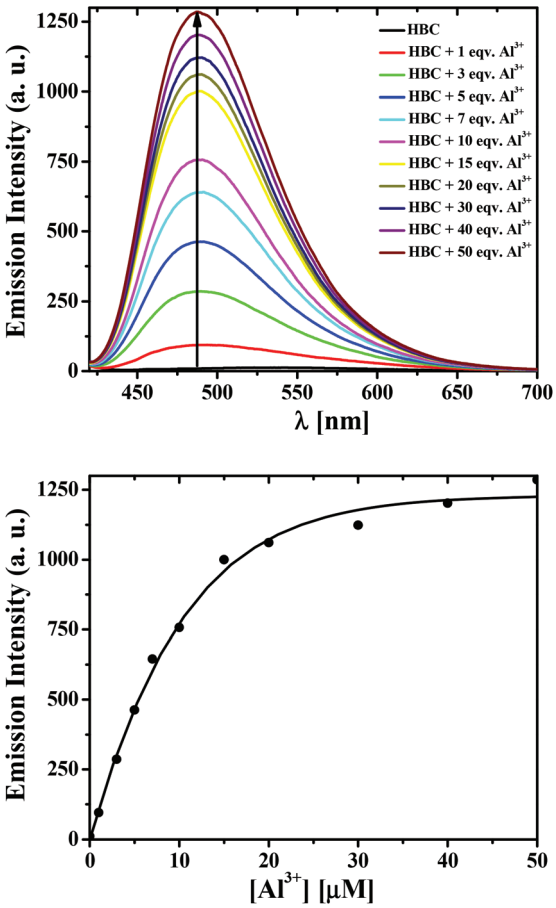

Fig. 5 Fluorescence spectra i of **HBC** (1 μM) upon addition of different equivalents of Al^{3+} (top). The plot of emission intensities of **HBC** as a function of added $[Al^{3+}]$ (bottom).

In order to characterize chelation from the qualitative and quantitative points of view, we have analyzed the bonding between **HBC** and the rest species **[Al(MeOH)(NO$_3$)$_3$]** based on the recently proposed charge and energy decomposition scheme ETS–NOCV (Fig. 6).[49]

First of all, an analysis of the most stable geometry of **[Al(HBC)(MeOH)(NO$_3$)$_3$]**, obtained from the BP86/TZP calculations, leads to the following conclusions: (*i*) the OH hydrogen of **HBC** has been transferred to the adjacent NO_3 unit (Fig. 6, A); (*ii*) **HBC** adopts a twisted conformation, which is similar to the isolated molecule (Fig. S8 in the ESI†). The former process makes the oxygen atom of the salicylaldehyde ring of **HBC** more nucleophilic, which facilitates donation from **HBC** to Al^{3+} and, accordingly, can result in the fluorescence enhancement due to the reduction of the intramolecular photoinduced electron transfer (PET).[50,51] Indeed, ETS–NOCV data allowed us to observe that donation of the lone electron pairs of oxygen and nitrogen atoms of **HBC** to the Al^{3+} center (characterized by $\Delta\rho_2$ and $\Delta\rho_3$) leads to a very high energetic stabilization $\Delta E_{orb}(2) + \Delta E_{orb}(3) = -74.4$ kcal mol^{-1} (Fig. 6, B). It is of comparable importance to the strength of a newly formed covalent O–H connection of the hydrogen bonding O_2NO–H···O(**HBC**), $\Delta\rho_1$ with the corresponding

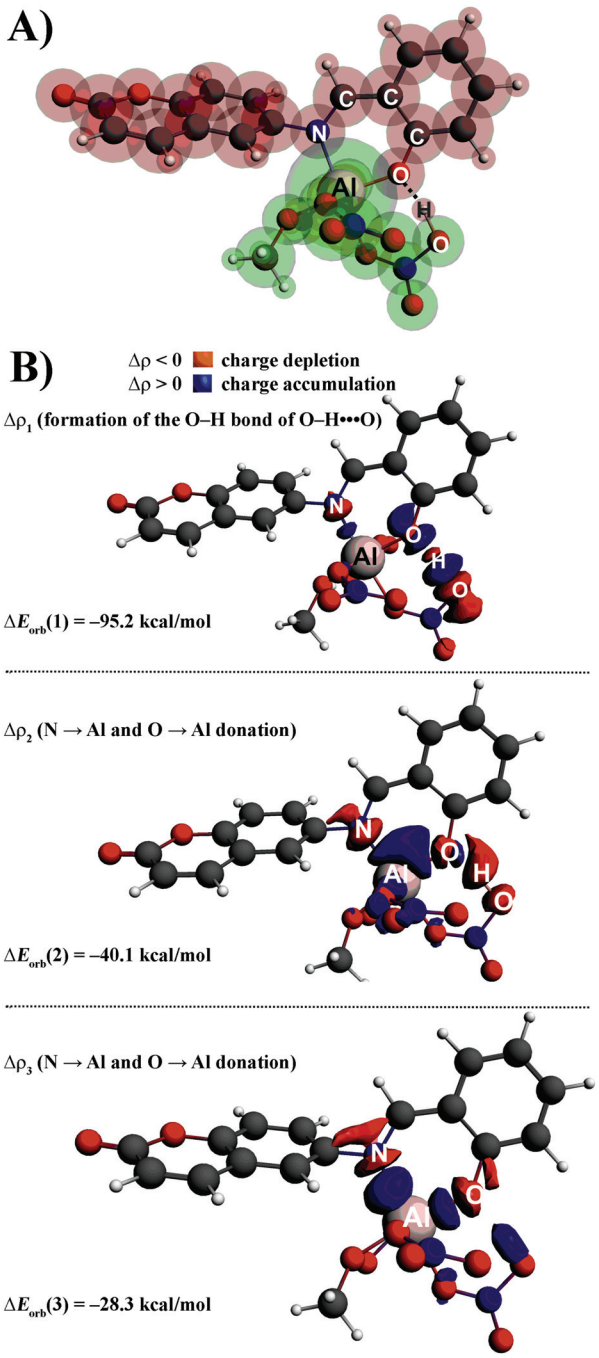

Fig. 6 ETS–NOCV based deformation density channels, $\Delta\rho_1$, $\Delta\rho_2$, $\Delta\rho_3$ (A) together with the corresponding energies, $\Delta E_{orb}(1)$, $\Delta E_{orb}(2)$, $\Delta E_{orb}(3)$, characterizing the chelation interaction in the **[Al(HBC)(MeOH)$(NO_3)_3$]** complex (B). Red and green shadows in part A show the way of fragmentation used in the ETS–NOCV analysis. The contour values are 0.003 a.u.

$\Delta E_{orb}(1) = -95.2$ kcal mol^{-1} (Fig. 6, B). One could also add that quenching of the fluorescence in non-complexed **HBC** can also be related to the deactivation of the excited state due to intramolecular proton transfer (Fig. S9 in the ESI†).[52]

Fig. 7 shows the Job's plot for the determination of the stoichiometry of [**HBC**-Al^{3+}] in aqueous MeOH. It is clearly observed that the Al^{3+} : **HBC** ratio is 1 : 1. The mass spectrum

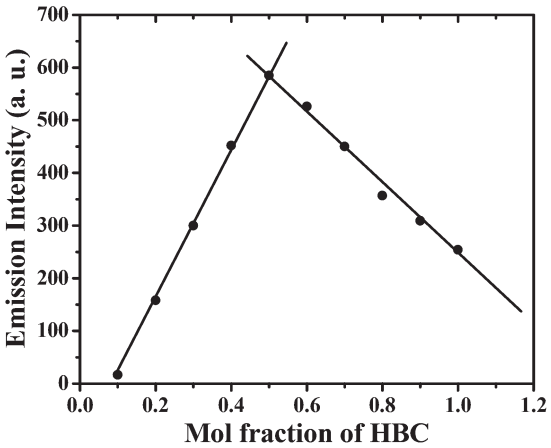

Fig. 7 Job's plot for the determination of the stoichiometry of [**HBC**-Al^{3+}] in H_2O–MeOH = 7 : 3 (v/v).

of the complex **[Al(HBC)(MeOH)$(NO_3)_3$]** (see the description above) also supports the found stoichiometry.

The fluorescence quantum yields of **HBC** and **[Al(HBC)(MeOH)$(NO_3)_3$]** were determined as Φ = 0.1% and 11.4%, respectively.

The binding constant of **HBC** with Al^{3+} has been determined using the Benesi–Hildebrand eqn (1) by the fluorescence method (Fig. 8).[53]

$$1/\Delta F = 1/\Delta F_{max} + (1/K[C]^n) \times (1/\Delta F_{max}) \quad (1)$$

here $\Delta F = (F_x - F_0)$ and $\Delta F_{max} = F_\infty - F_0$, where F_0, F_x, and F_∞ are the emission intensities of **HBC** in the absence of Al^{3+}, at an intermediate Al^{3+} concentration, and at a concentration of the complete interaction, respectively. K is the binding constant, C is the concentration of Al^{3+} and n is the number of Al^{3+} ions bound to each **HBC** (here n = 1).

The value of K, as obtained from the slope, is 7.9×10^4 M^{-1}. A linear regression curve was then fitted to the normalized

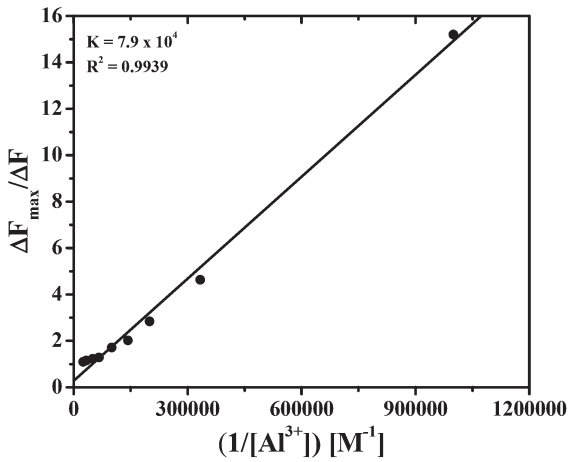

Fig. 8 Determination of the binding constant of **HBC** (10 μM) with Al^{3+} (10 μM) in H_2O–MeOH = 7 : 3 (v/v) using the Benesi–Hildebrand equation by the fluorescence method.

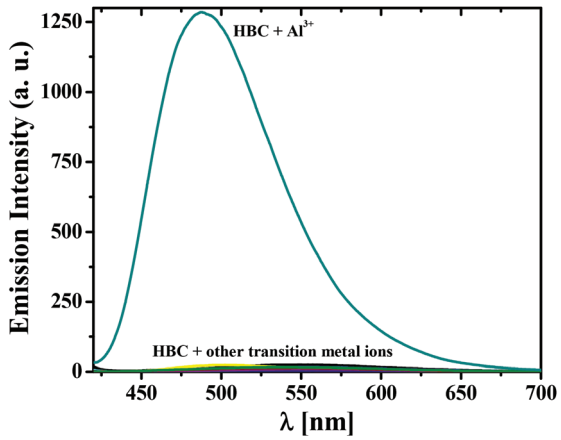

Fig. 9 Emission intensities of **HBC** (1 μM) in the presence of different metal ions (10 μM) in H_2O–MeOH = 7 : 3 (v/v).

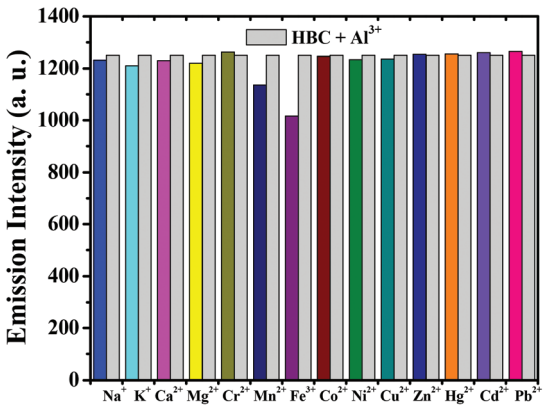

Fig. 10 Interference of different metal ions in the determination of $[Al^{3+}]$ (10 μM) with **HBC** (1 μM) and foreign alkali, alkaline earth and transition metal ions (100 μM).

fluorescence intensity data and the point at which this line crossed the ordinate axis has been considered as the detection limit. **HBC** could detect as low as 0.5 μM of Al^{3+} in aqueous MeOH.

The selectivity of **HBC** towards Al^{3+} over other common accompanying metal ions was examined in aqueous MeOH solutions. Fig. 9 clearly indicates that only Al^{3+} enhances the fluorescence intensity of **HBC**.

This unique selectivity of **HBC** towards Al^{3+} can be interpreted in terms of the absolute hardness (η), defined as $\eta = (I + A)/2$, where I and A are the ionization potential and proton affinity, respectively. Namely, it was reported by Paar and Pearson that Al^{3+} is the hardest acid among all of the cations considered in this study.[54] This allows a strong coordination ability between **HBC** and Al^{3+}, which can lead to the effective (**HBC**)N,O → Al^{3+} donation and accordingly to fluorescence enhancement. We have further calculated, based on the DFT/BP86/TZP method, the total interaction energies between the selected cations and **HBC** (Table S1 in ESI†). It has been found, in line with the picture originating from the hardness parameter, that **HBC** is by far the strongest bonded to Al^{3+} (Table S1 in the ESI†). The ETS–NOCV method allowed us to observe that it is indeed predominantly due to the lowest orbital interaction term, determined by the (**HBC**)N,O → Al^{3+} donation (Fig. S10 and Table S1 in the ESI†).

Studies on the interferences of common alkali, alkaline earth and transition metal ions in the emission intensity of the [**HBC**-Al^{3+}] system are presented in Fig. 10. An increase in fluorescence intensity of the [**HBC**-Al^{3+}] system upon addition of a foreign ion was designated as positive interference, whereas the reverse phenomenon was termed as negative interference. Fe^{3+} and Mn^{2+} show insignificant negative interference.

Al^{3+} treated and untreated cells have been mixed with **HBC** and observed under a fluorescence microscope. Fig. 11 shows that **HBC** can easily permeate to the tested living cells with no harm as the cells remain alive even after a 0.5 h exposure to **HBC** (1 μM). *Bacillus* sp., which is widely used as a bio-pesticide for controlling looper killer at tea plantations, have been grown from 24 h culture medium and treated with an aqueous solution of Al^{3+} (1 mg mL^{-1}) for 1 h, washed with normal saline and observed under a fluorescence microscope after adding **HBC**. **HBC** treated cells without any externally added Al^{3+} have been used as a control.

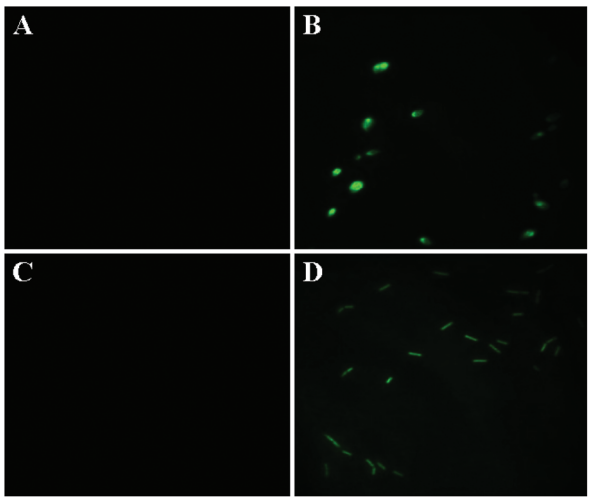

Fig. 11 Fluorescence microscopic images of *Bacillus* sp. and *Candida* sp. (*Candida albicans*) cells treated with **HBC** (1 μM): images in the absence (A and C) and presence (B and D) of Al^{3+} (incubation temperature is 40 °C).

Crystals of **HBC** were obtained by slow evaporation of the solvent from its MeOH solution. The molecular structure is shown in Fig. 12, while the crystal and structure refinement data are given in the Experimental section.

The compound **HBC** crystallizes in the triclinic space group $P\bar{1}$ and contains two independent molecules in the asymmetric unit cell. Each molecule is found in the enolimine form (Fig. 12). The bond lengths of C(12)–O(1) and C(12A)–O(1A) are 1.354(4)–1.364(4) Å and those of N(1)–C(2) and N(1A)–C(2A) are 1.426(4)–1.440(4) Å, which indicate single bonds, whereas a double bond is revealed from N(1)═C(1) and N(1A)═C(1A) being 1.264(5)–1.289(4) Å (Table S2 in the ESI†). Furthermore,

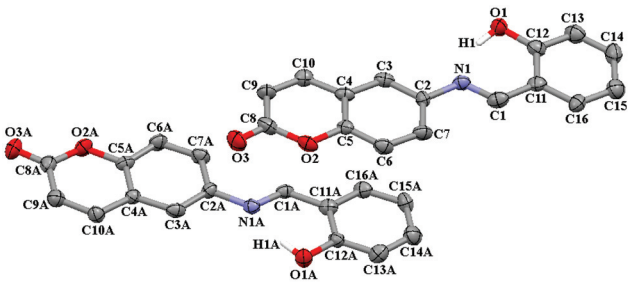

Fig. 12 Thermal ellipsoid (50%) plot of molecule A (top) and molecule B (bottom) of **HBC**. H-atoms, not involved in hydrogen bonding, are omitted.

the bond angles C(1)═N(1)–C(2) and C(1A)═N(1A)–C(2A) are 120.9(3)–121.0(3)°, indicating the sp^2-hybridization of the nitrogen atoms (Table S2 in the ESI†). Molecules of **HBC** are found to be completely planar with torsion angles N(1)–C(1)–C(11)–C(12) and N(1A)–C(1A)–C(11A)–C(12A) being −179.9(3) and 0.3(5)°, respectively, and dihedral angles Φ between aromatic rings of 5.48(17) and 2.73(2)°, respectively. The crystal structure of **HBC** is stabilized by the intramolecular hydrogen bond of the type O–H···N, which is formed between the hydrogen atom of the OH group and the nitrogen atom of the imine group (Fig. 12, Table S2 in the ESI†). Moreover, molecules of **HBC** are perfectly stacked in the crystal packing (Fig. 13). The energy decomposition analysis (ETS)[55] indicated that **HBC** units in the crystal structure are weakly bonded (the total interaction energy is −11.42 kcal mol^{-1}) predominantly by the dispersion forces (Table S4 in the ESI†).

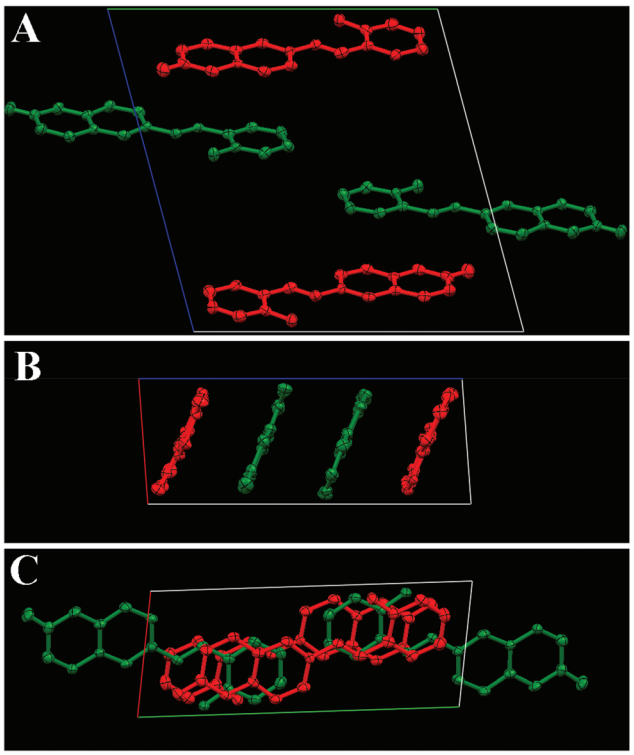

Fig. 13 Thermal ellipsoid (50%) plot of the crystal packing of **HBC** along the 0*a* (A), 0*b* (B) and 0*c* (C) axes. Molecule A and molecule B are given in red and green, respectively. H-atoms are omitted.

Conclusions

In summary, a comparison of the present probe with other existing Al^{3+} sensitive "turn-on" fluorescent probes reveals that it is very competitive and somewhat better than others in respect of all the parameters. The present probe is less expensive as it involves a facile one step reaction with commercially available much cheaper chemicals. Its structure has been confirmed by a single crystal X-ray analysis. Coumarin being a bioactive molecule, the use of its derivative (**HBC**) for living cell imaging will be more effective and justified.

Experimental

Materials and methods

Salicylaldehyde and coumarin have been purchased from Aldrich (USA) and S. D. Fine Chem. Ltd (India), respectively. 6-Aminocoumarin is synthesized starting from coumarin by following a published procedure.[56] Analytical grade chemicals and spectroscopy grade solvents are used. Milli-Q 18.2 MΩ cm^{-1} water is used throughout all the experiments. The sources of Mn^{2+}, Cr^{3+}, Fe^{3+}, Co^{2+}, Ni^{2+}, Cu^{2+}, Zn^{2+}, Cd^{2+}, Hg^{2+} and Pb^{2+} ions are either their chloride, nitrate or perchlorate salts.

Physical measurements

IR spectra in KBr are recorded on a Perkin Elmer FTIR spectrometer (model: RX-1). ^{1}H NMR spectra in D_2O–CD_3OD = 7 : 3 (v/v) are recorded with a Bruker Avance 300 MHz using tetramethylsilane as an internal standard. Absorption and fluorescence spectra in aqueous MeOH (H_2O–MeOH = 7 : 3, v/v) are recorded with a Shimadzu Multi Spec 1501 spectrophotometer and a Hitachi F-4500 fluorescence spectrometer, respectively. Mass spectra are recorded with a QTOF Micro YA 263 mass spectrometer in the ESI positive mode. pH measurements are performed with a Systronics digital pH meter (model 335). The fluorescence imaging system is comprised of an inverted fluorescence microscope (Leica DM 1000 LED), a digital compact camera (Leica DFC 420C) and an image processor (Leica Application Suite v3.3.0). The microscope is equipped with a 50 W mercury arc lamp. Elemental analyses are performed on a Perkin Elmer 2400 CHNS/O elemental analyzer.

Quantum yield measurements

The fluorescence quantum yields have been determined using anthracene as a reference with a known ϕ_R value of 0.2 in MeOH.[57] The sample and the reference dye are excited at the same wavelength (λ_{ex} = 350 nm), maintaining nearly equal absorbance (0.1) and emission spectra. The area of the emission spectrum is integrated using the software available in the instrument and the quantum yield is calculated according to

the following equation:

$$\phi_S/\phi_R = [A_S/A_R] \times [(Abs)_R/(Abs)_S] \times [\eta_S{}^2/\eta_R{}^2]$$

where ϕ_S and ϕ_R are the fluorescence quantum yields of the sample and the reference, respectively; A_S and A_R are the area under the fluorescence spectra of the sample and the reference, respectively; $(Abs)_S$ and $(Abs)_R$ are the corresponding optical densities of the sample and the reference solution at the wavelength of excitation; η_S and η_R are the refractive indexes of the sample and the reference, respectively.

The ETS–NOCV method

Historically, the natural orbitals for chemical valence (NOCV) have been derived from the Nalewajski–Mrozek valence theory as eigenvectors that diagonalize the deformation density matrix. It is shown that the natural orbitals for chemical valence pairs (ψ_{-k}, ψ_k) decompose the differential density $\Delta\rho$ into NOCV-contributions ($\Delta\rho_k$):

$$\Delta\rho(r) = \sum_{k=1}^{M/2} \nu_k[-\psi^2_{-k}(r) + \psi^2_k(r)] = \sum_{k=1}^{M/2} \Delta\rho_k(r)$$

where ν_k and M stand for the NOCV eigenvalues and the number of basis functions, respectively. Visual inspection of deformation density plots ($\Delta\rho_k$) helps us to attribute the symmetry and the direction of the charge flow. In addition, these pictures are enriched by providing the energetic estimations, $\Delta E_{orb}(k)$, for each $\Delta\rho_k$ within the ETS–NOCV scheme. The exact formula which links the ETS and NOCV methods will be given in the next paragraph after we briefly present the basic concept of the ETS scheme. In this method, the total bonding energy ΔE_{total} between interacting fragments exhibiting the geometry as in the combined complex is divided into three components: $\Delta E_{total} = \Delta E_{elstat} + \Delta E_{Pauli} + \Delta E_{orb}$.

The first term, ΔE_{elstat}, corresponds to the classical electrostatic interaction between the promoted fragments as they are brought to their positions in the final complex. The second term, ΔE_{Pauli}, accounts for the repulsive Pauli interaction between occupied orbitals on the two fragments in the combined molecule. Finally, the last stabilizing term, ΔE_{orb}, represents the interactions between the occupied molecular orbitals of one fragment and the unoccupied molecular orbitals of the other fragment as well as the mixing of occupied and virtual orbitals within the same fragment (inner-fragment polarization). This energy term may be linked to the electronic bonding effect coming from the formation of a chemical bond. The three last terms (ΔE_{elstat}, ΔE_{Pauli}, and ΔE_{orb}) very often are combined into the instantaneous interaction energy, ΔE_{int}, as it describes the interaction between the fragments in the geometry of the complex.

In the combined ETS–NOCV scheme,[49] the orbital interaction term (ΔE_{orb}) is expressed in terms of NOCV's eigenvalues (ν_k) as:

$$\Delta E_{orb} = \sum_k \Delta E_{orb}(k) = \sum_{k=1}^{M/2} \nu_k[-F^{TS}_{-k,-k} + F^{TS}_{k,k}]$$

where $F^{TS}_{i,i}$ are diagonal Kohn–Sham matrix elements defined over NOCV with respect to the transition state (TS) density (at the midpoint between the density of the molecule and the sum of fragment densities). Components $\Delta E_{orb}(k)$ provide the energetic estimation of $\Delta\rho_k$ that may be related to the importance of a particular electron flow channel for the bonding between the considered molecular fragments. ETS–NOCV analysis was done based on the Amsterdam Density Functional (ADF) package in which this scheme was implemented.[47,48]

Synthesis of HBC. 6-Aminocoumarine (0.5 g, 3.1 mmol) and salicylaldehyde (0.378 g, 3.1 mmol) in MeOH (15 mL) have been refluxed for 8 h. Slow evaporation of the solvent has yielded a yellow crystalline compound. Yield: 0.740 g (90%). m.p. 140 ± 2 °C. FTIR, ν: 1624 (C═N), 1724 (C═O), 3427 (OH) cm^{-1}. ^1H NMR, δ: 6.44 (d, $^3J_{H,H}$ = 9.9 Hz, 1H, aryl), 6.93–7.13 (m, 4H, aryl), 7.25 (d, $^3J_{H,H}$ = 9.2 Hz, 1H, aryl), 7.58 (t, $^3J_{H,H}$ = 8.4 Hz, 1H, aryl), 7.71 (d, $^3J_{H,H}$ = 7.7 Hz, 1H), 7.92 (d, $^3J_{H,H}$ = 9.5 Hz, 1H), 9.97 (s, 1H, CHN) ppm. UV-Vis, λ_{max} ($\varepsilon \times 10^3$, M^{-1} cm^{-1}): 240 (425), 277 (310), 318 (sh., 84), 347 (99) nm. QTOF-MS ES^+, m/z (I, %): 266.05 (100) $[M + Na]^+$. Anal. Calc. for $C_{16}H_{11}NO_3$ (265.27): C 72.45, H 4.18, N 5.28. Found: C 72.18, H 4.13, N 5.26%.

Synthesis of [Al(HBC)(MeOH)$(NO_3)_3$]. $Al(NO_3)_3{\cdot}9H_2O$ (0.025 g, 0.067 mmol) in MeOH (10 mL) is slowly added to a magnetically stirred solution of **HBC** (0.035 g, 0.067 mmol) in the same solvent (10 mL). The mixture is stirred for 0.5 h. Then the solvent is evaporated to obtain a yellow compound. FTIR, ν: 1385 (NO_3), 1615 (C═N), 1724 (C═O), 3072 (OH, MeOH), 3423 (OH) cm^{-1}. ^1H NMR, δ: 6.32 (d, $^3J_{H,H}$ = 9.8 Hz, 1H, aryl), 6.88–7.12 (m, 4H, aryl), 7.31 (d, $^3J_{H,H}$ = 9.0 Hz, 1H, aryl), 7.59 (t, $^3J_{H,H}$ = 8.3 Hz, 1H, aryl), 7.74 (d, $^3J_{H,H}$ = 7.8 Hz, 1H), 8.02 (d, $^3J_{H,H}$ = 9.6 Hz, 1H), 10.32 (s, 1H, CHN), 13.17 (s, 1H, OH) ppm. UV-Vis, λ_{max} ($\varepsilon \times 10^3$, M^{-1} cm^{-1}): 240 (425), 275 (276), 321 (50), 375 (53) nm. QTOF-MS ES^+, m/z (I, %): 162.09 (15) [6-aminocoumarin + H]$^+$, 184.08 (13) [6-aminocoumarin + Na]$^+$, 266.12 (93) [HBC + H]$^+$, 288.10 (100) [HBC + Na]$^+$, 304.08 (9) [HBC + K]$^+$, 449.20 (4) $[M - NO_3]^+$, 533.19 (50) [M + Na]$^+$. Anal. Calc. for $C_{17}H_{15}AlN_4O_{13}$ (510.31): C 40.01, H 2.96, N 10.98. Found: C 40.00, H 3.08, N 10.16%.

Measurement procedures

Solutions of Al^{3+} and **HBC** are prepared by dissolving the corresponding amounts of $Al(NO_3)_3$ and **HBC** in aqueous MeOH (H_2O–MeOH = 7 : 3, v/v). Solutions of Al^{3+} and **HBC** are mixed in different ratios in different sets for subsequent UV-Vis and fluorescence measurements using a 1 cm quartz cell.

X-ray crystallography

The X-ray data of **HBC** are collected at 173(2) K on a STOE IPDS-II diffractometer with graphite-monochromatised Mo-K_α radiation generated by a fine-focus X-ray tube operated at 50 kV and 40 mA. The reflections of the images are indexed, integrated and scaled using the X-Area data reduction package.[58] Data are corrected for absorption using the PLATON program.[59] The structure is solved by a direct method

using the SHELXS-97 program[60] and refined first isotropically and then anisotropically using SHELXL-97.[60] Hydrogen atoms are revealed from $\Delta\rho$ maps and those bonded to C are refined using appropriate riding models. The hydrogen atom bonded to N is freely refined. Figures are generated using the Mercury program.[61] $C_{16}H_{11}NO_3$, M_r = 265.26 g mol^{-1}, triclinic, space group $P\bar{1}$, a = 5.7162(10), b = 15.008(3), c = 15.078(2) Å, α = 74.238(12), β = 83.545(13), γ = 80.741(14)°, V = 1225.4(4) Å^3, Z = 4, ρ = 1.438 g cm^{-3}, μ(Mo-Kα) = 0.101 mm^{-1}, reflections: 16 166 collected, 16 166 unique, R_{int} = 0.0000, R_1(all) = 0.1470, wR_2(all) = 0.2091.

CCDC 857625 contains the supplementary crystallographic data.

Acknowledgements

Financial support from UGC-DAE-Kolkata Center is gratefully acknowledged. A. Sahana and S. Lohar are thankful to CSIR, New Delhi for providing fellowships. We convey our sincere thanks to USIC, Burdwan University for extending the facility of a fluorescence microscope. This work was also funded by the Fonds National de la Recherche Scientifique-FNRS (FRFC No 2.4508.08). D. A. Safin and M. B. Babashkina thank WBI (Belgium) for post-doctoral positions. M. P. Mitoraj acknowledges the financial support from the Polish Ministry of Science and Higher Education ("Outstanding Young Researchers" scholarship, 2011–2014), the National Science Center in Poland (grant no. N204 198040) and the computational support from PL-Grid Infrastructure.

Notes and references

1 E. Delhaize and P. R. Ryan, *Plant Physiol.*, 1995, **107**, 315.
2 D. R. Crapper McLachlan, W. J. Lukiw and T. P. A. Kruck, *Environ. Geochem. Health*, 1990, **12**, 103.
3 B. Valeur and I. Leray, *Coord. Chem. Rev.*, 2000, **205**, 3.
4 T. P. Flaten, *Brain Res. Bull.*, 2001, **55**, 187.
5 J. R. Walton, *Curr. Inorg. Chem.*, 2012, **2**, 19.
6 G. C. Woodson, *Bone*, 1998, **22**, 695.
7 P. D. Darbre, *J. Inorg. Biochem.*, 2005, **99**, 1912.
8 G. D. Fasman, *Coord. Chem. Rev.*, 1996, **149**, 125.
9 M. Sargazi, N. B. Roberts and A. J. Shenkin, *Inorg. Biochem.*, 2001, **87**, 37.
10 M. I. Yousef, A. M. EI-Morsy and M. S. Hassan, *Toxicology*, 2005, **215**, 97.
11 M. G. Sont, S. M. White, W. G. Flamm and G. A. Burdock, *Regul. Toxicol. Pharmacol.*, 2001, **33**, 66.
12 N. W. Bavlor, W. Egan and P. Richman, *Vaccine*, 2002, **20**, S18.
13 C. J. Exley, *Inorg. Biochem.*, 2005, **99**, 1747.
14 K. Soroka, R. S. Vithanage, D. A. Phillips, B. Walker and P. K. Dasgupta, *Anal. Chem.*, 1987, **59**, 629.
15 F. Launay, V. Alain, E. Destandau, N. Ramos, E. Bardez, P. Baret and J. L. Pierre, *New J. Chem.*, 2001, **25**, 1269.
16 A. W. Czarnik, *Fluorescent Chemosensors for Ion and Molecule Recognition*, ACS Symposium Series No. 538. American Chemical Society, Washington, 1992.
17 *Chemosensors for Ion and Molecule Recognition*, ed. J. P. Desvergne and A. W. Czarnik, Kluwer, Boston, 1997.
18 E. Bakker, P. Buhlmann and E. Pretsch, *Chem. Rev.*, 1997, **97**, 3083.
19 L. Salmon, P. Thuery, E. Riviere and M. Ephritikhine, *Inorg. Chem.*, 2006, **45**, 83.
20 V. C. Da Silveira, J. S. Luz, C. C. Oliveira, I. Graziani, M. R. Ciriolo and A. M. Ferreira, *J. Inorg. Biochem.*, 2008, **102**, 1090.
21 S. Padhye and G. B. Kauffman, *Coord. Chem. Rev.*, 1985, **63**, 127.
22 S. Kasselouri, A. Garoufis, A. Katehanakis, G. Kalkanis, S. P. Perlepes and N. Hadjiliadis, *Inorg. Chim. Acta*, 1993, **207**, 255.
23 J. M. Cano-pavón, M. L. Trujillo and A. García De Torres, *Anal. Chim. Acta*, 1980, **117**, 319.
24 C. Jiang, B. Tang, R. Wang and J. Yen, *Talanta*, 1997, **44**, 197.
25 D. Maity and T. Govindaraju, *Chem. Commun.*, 2012, **48**, 1039.
26 D. Maity and T. Govindaraju, *Eur. J. Inorg. Chem.*, 2011, 5479.
27 F. Pablos, J. L. G. Ariza and F. Pino, *Analyst*, 1986, **111**, 1159.
28 D. Karak, S. Lohar, A. Sahana, S. Guha, A. Banerjee and D. Das, *Anal. Methods*, 2012, **4**, 1906.
29 M. P. Manuel-Vez and M. Garcia-Vargas, *Talanta*, 1994, **41**, 1553.
30 M. S. J. Briggs, J. S. Fossey, C. J. Richards, B. Scotta and J. Whately, *Tetrahedron Lett.*, 2002, **43**, 5169.
31 M. Arduini, F. Felluga, F. Mancin, P. Rossi, P. Tecilla, U. Tonellato and N. Valentinuzzi, *Chem. Commun.*, 2003, 1606.
32 D. Maity and T. Govindaraju, *Chem. Commun.*, 2010, **46**, 4499.
33 A. B. Othman, J. W. Lee, Y. D. Huh, R. Abidi, J. S. Kimd and J. Vicens, *Tetrahedron*, 2007, **63**, 10793.
34 Y. W. Wang, M. X. Yu, Y. H. Yu, Z. P. Bai, Z. Shen, F. Y. Li and X. Z. You, *Tetrahedron Lett.*, 2009, **50**, 6169.
35 R. S. Sathish, A. G. Raju, G. N. Rao and C. Janardhana, *Spectrochim. Acta, Part A*, 2008, **69**, 282.
36 Y. Zhao, Z. Lin, H. Liao, C. Duan and Q. Meng, *Inorg. Chem. Commun.*, 2006, **9**, 966.
37 A. Jeanson and V. Bereau, *Inorg. Chem. Commun.*, 2006, **9**, 13.
38 D. Maity and T. Govindaraju, *Inorg. Chem.*, 2010, **49**, 7229.
39 Y. Lu, S. Huang, Y. Liu, S. He, L. Zhao and X. Zeng, *Org. Lett.*, 2011, **13**, 5274.
40 A. Sahana, A. Banerjee, S. Das, S. Lohar, D. Karak, B. Sarkar, S. K. Mukhopadhyay, A. K. Mukherjee and D. Das, *Org. Biomol. Chem.*, 2011, **9**, 5523.
41 L. Wang, W. Qin, X. Tang, W. Dou, W. Liu, Q. Teng and X. Yao, *Org. Biomol. Chem.*, 2010, **8**, 3751.

42 C. Gou, S.-H. Qin, H.-Q. Wu, Y. Wang, J. Luo and X.-Y. Liu, *Inorg. Chem. Commun.*, 2011, **14**, 1622.
43 E. Oliveira, H. M. Santos, J. L. Capelo and C. Lodeiro, *Inorg. Chim. Acta*, 2012, **381**, 203.
44 X.-H. Jiang, B.-D. Wang, Z.-Y. Yang, Y.-C. Liu, T.-R. Li and Z.-C. Liu, *Inorg. Chem. Commun.*, 2011, **14**, 1224.
45 A. Banerjee, A. Sahana, S. Das, S. Lohar, S. Guha, B. Sarkar, S. K. Mukhopadhyay, A. K. Mukherjee and D. Das, *Analyst*, 2012, **137**, 2166.
46 S. Das, A. Sahana, A. Banerjee, S. Lohar, D. A. Safin, M. G. Babashkina, M. Bolte, Y. Garcia, I. Hauli, S. K. Mukhopadhyayd and D. Das, *Dalton Trans.*, 2013, **42**, 4757.
47 G. te Velde, F. M. Bickelhaupt, E. J. Baerends, C. Fonseca Guerra, S. J. A. van Gisbergen, J. G. Snijders and T. Ziegler, *J. Comput. Chem.*, 2001, **22**, 931 and references therein.
48 E. J. Baerends, J. Autschbach, D. Bashford, A. Bérces, F. M. Bickelhaupt, C. Bo, P. M. Boerrigter, L. Cavallo, D. P. Chong, L. Deng, R. M. Dickson, D. E. Ellis, M. van Faassen, L. Fan, T. H. Fischer, C. Fonseca Guerra, A. Ghysels, A. Giammona, S. J. A. van Gisbergen, A. W. Götz, J. A. Groeneveld, O. V. Gritsenko, M. Grüning, F. E. Harris, P. van den Hoek, C. R. Jacob, H. Jacobsen, L. Jensen, G. van Kessel, F. Kootstra, M. V. Krykunov, E. van Lenthe, D. A. McCormack, A. Michalak, M. Mitoraj, J. Neugebauer, V. P. Nicu, L. Noodleman, V. P. Osinga, S. Patchkovskii, P. H. T. Philipsen, D. Post, C. C. Pye, W. Ravenek, J. I. Rodríguez, P. Ros, P. R. T. Schipper, G. Schreckenbach, M. Seth, J. G. Snijders, M. Solà, M. Swart, D. Swerhone, G. te Velde, P. Vernooijs, L. Versluis, L. Visscher, O. Visser, F. Wang, T. A. Wesolowski, E. M. van Wezenbeek, G. Wiesenekker, S. K. Wolff, T. K. Woo, A. L. Yakovlev and T. Ziegler, *Theoretical Chemistry*, Vrije Universiteit, Amsterdam, ADF2009.01.
49 M. Mitoraj, A. Michalak and T. Ziegler, *J. Chem. Theory Comput.*, 2009, **5**, 962.
50 A. Prasanna de Silva, T. S. Moody and G. D. Wright, *Analyst*, 2009, **134**, 2385.
51 K. Sasamoto, T. Ushijima, M. Sato and Y. Ohkura, *Anal. Sci.*, 1996, **12**, 189.
52 A. Maliakal, G. Lem, N. J. Turro, R. Ravichandran, J. C. Suhadolnik, A. D. DeBellis, M. G. Wood and J. Lau, *J. Phys. Chem. A*, 2002, **106**, 7680 and references therein.
53 H. A. Benesi and J. H. Hildebrand, *J. Am. Chem. Soc.*, 1949, **71**, 2703.
54 R. G. Paar and R. G. Pearson, *J. Am. Chem. Soc.*, 1983, **105**, 7512.
55 T. Ziegler and A. Rauk, *Theor. Chim. Acta*, 1977, **46**, 1.
56 S. Guha, S. Lohar, M. Bolte, D. A. Safin and D. Das, *Spectrosc. Lett.*, 2012, **45**, 225.
57 W. H. Melhuish, *J. Phys. Chem.*, 1961, **65**, 229.
58 Stoe & Cie, *X-AREA. Area-Detector Control and Integration Software*, Stoe & Cie, Darmstadt, Germany, 2001.
59 A. L. Spek, *Acta Crystallogr., Sect. D: Biol. Crystallogr.*, 2009, **65**, 148.
60 G. M. Sheldrick, *Acta Crystallogr., Sect. A: Fundam. Crystallogr.*, 2008, **64**, 112.
61 I. J. Bruno, J. C. Cole, P. R. Edgington, M. Kessler, C. F. Macrae, P. McCabe, J. Pearson and R. Taylor, *Acta Crystallogr., Sect. B: Struct. Sci.*, 2002, **58**, 389.